PCCP

Accepted Manuscript

ROYAL SOCIETY OF CHEMISTRY

www.rsc.org/pccp

Configuration coordinate energy level diagrams of intervalence and metal-to-metal charge transfer states of dopant pairs in solids.

Zoila Barandiarán,[1,2] Andries Meijerink,[3] and Luis Seijo[1,2]

[1]*Departamento de Química, Universidad Autónoma de Madrid, 28049 Madrid, Spain*
[2]*Instituto Universitario de Ciencia de Materiales Nicolás Cabrera, Universidad Autónoma de Madrid, 28049 Madrid, Spain*
[3]*Condensed Matter and Interfaces, Debye Institute for Nanomaterials Science, Utrecht University, Princetonplein 5, 3584 CC Utrecht, The Netherlands*

(Dated: June 23, 2015)

Configuration coordinate diagrams, which are normally used in a qualitative manner for the energy levels of active centers in phosphors, are quantitatively obtained here for intervalence charge transfer (IVCT) states of mixed valence pairs and metal-to-metal charge transfer (MMCT) states of heteronuclear pairs, in solid hosts. The procedure relies on vibrational frequencies and excitation energies of single-ion active centers, and on differences between ion-ligand distances of donor and acceptor, which are attainable empirically or in *ab initio* calculations. The configuration coordinate diagrams of the Yb^{2+}/Yb^{3+} mixed-valence pair in Yb-doped YAG and the Ce^{3+}/Yb^{3+} heteronuclear pair in Ce,Yb-codoped YAG, are obtained and described. They are drawn from empirical data of the single-ions and their usefulness is discussed. The first diagram suggests that IVCT states of Yb^{2+}/Yb^{3+} pairs may play an important role in the quenching of the Yb^{3+} emission and it provides the details of the quenching mechanism. The second diagram supports the interpretation recently given for the energy transfer from Ce^{3+} to Yb^{3+} in Ce,Yb-codoped YAG via a MMCT Ce^{4+}-Yb^{2+} state and it provides the details. The analyses of the two diagrams suggest the formation of Yb^{2+}/Yb^{3+} pairs after the Ce^{3+}-to-Yb^{3+} MMCT as responsible for the temperature quenching of the Yb^{3+} emission excited with $Ce^{3+}(4f \rightarrow 5d)$ absorption in Ce,Yb-codoped YAG.

Keywords: MMCT, IVCT, Ce, Yb, YAG, concentration quenching, temperature quenching, energy transfer

I. INTRODUCTION

Electron transfer between two metal ions involved in a redox process is an important phenomenon in biology, chemistry, and material science. It is often known as metal-to-metal charge transfer (MMCT). When the two metal ions differ only in oxidation state, the conventional name of this process is intervalence charge transfer (IVCT).[1] [The term IVCT is used sometimes for MMCT between non-equivalent metal ions and also for electron transfer processes not involving metals; here we will adopt the conventional meaning and we will call IVCT only to the homonuclear, symmetric MMCT.]

MMCT states are considered to have an important role in energy transfer processes between optically active centers of doped solids and in non-radiative decays which can drastically change the optical behavior of materials.[2] The blue to near-infrared conversion in Ce^{3+},Yb^{3+}-codoped YAG (Ref. 3) and the ultaviolet to greenish-blue or to red conversions in Pr^{3+}-doped $CaTiO_3$ and $CaZrO_3$ (Ref. 4) are respective examples.

IVCT absorptions, which have been found in a large number of mixed-valence molecular compounds,[5,6] have also been reported in lanthanide activated phosphors like Ce^{3+}-doped $LaPO_4$ (Ref. 7), and lanthanide mixed-valence solids like $Na_5Eu_7Cl_{22}$ (Ref. 8). And IVCT luminescence has recently been reported to exist as well, and to be responsible for the anomalous emissions of Ce^{3+} in elpasolites[9] and Yb^{2+} in fluorites.[10] In fact, the IVCT states of mixed-valence pairs in doped solids have a high potential for changing the absorptions, emissions, and non-radiative decays of the materials when the pairs are formed, because these states are intercalated between the regular states of single-ion active centers.[9,10] Hence the importance of a detailed knowledge of the IVCT states in materials where such mixed-valence pairs are likely to form. Among others, this could be the case of solids activated with Ce^{3+}, Pr^{3+}, Eu^{2+}, or Yb^{2+} lanthanide dopants, in which preventing the coexistence of several valence states is difficult.[11,12]

It is common to address the participation of MMCT and IVCT states in energy transfer, non-radiative decay, and radiative processes with the help of schematic configuration coordinate energy level diagrams[2–4,7] (cf. Fig. 4 in Ref. 7, for instance). Here, we present an alternative to make quantitative IVCT and MMCT configuration coordinate diagrams using structural and energetic data of the single-ion active centers, which are attainable empirically or in *ab initio* calculations. We discuss their meaning and use as interpretative tools for the issues mentioned above.

As bases for the elaboration of the IVCT and MMCT configuration coordinate diagrams, we take the vibronic model for the IVCT absorption of the two-state problem of a mixed-valence pair of Piepho *et al.*[13] and its extension to excited states, which was used to analyze state-of-the-art *ab initio* calculations of the diabatic potential energy surfaces of Ce^{3+}/Ce^{4+} and Yb^{2+}/Yb^{3+} pairs of dopant ions in solids.[9,10] The latter revealed that, even though adiabatic potential energy surfaces calculated with a full consideration of electronic couplings between electronic states of donor and acceptor centres are necessary for IVCT absorption and emission intensities and non-radiative decay rates, a great deal of quantitative spectroscopic information on the pairs can be attained at the diabatic level, i.e. without explicit consid-

eration of donor-acceptor electronic couplings. Hence, we focus here on the diabatic approximation to configuration coordinate diagrams.

We discuss the definition of the configuration coordinate of a single-ion active center and its corresponding energy level diagram in Sec. II. This serves as a basis for the definition of the IVCT configuration coordinate of a mixed-valence pair in Sec. III, where the corresponding energy level diagram is discussed. The same is done for the MMCT states of a heteronuclear metalic pair in Sec. IV. Detailed discussions of IVCT and MMCT sample cases are given: Yb^{2+}/Yb^{3+} mixed-valence pair in YAG, Sec. III B, and Ce^{3+}/Yb^{3+} heteronuclear pair in YAG, Sec. IV B.

II. CONFIGURATION COORDINATE OF A SINGLE ION ACTIVE CENTER

Let us briefly discuss on the configuration coordinate of a single ion active center and its corresponding configuration coordinate diagram. This diagram is a very useful simplified representation of the variation in energy of the electronic levels of the active center with the nuclear displacements. In this simplified description, only one vibrational coordinate is used, which is called the configuration coordinate, and the diagram is aimed at providing gross details of the crossings and relative positions of the electronic levels. Fine details, such as Jahn-Teller distortions, demand the use of several vibrational coordinates.

Let us consider the energies of the electronic levels of an optically active center with a single ion in the absence of (Jahn-Teller) vibronic couplings between degenerate states. The potential energy surface of the active center in its ground state can be written as a function of its normal vibrational coordinates as:

$$E_0(Q_1,Q_2,\ldots)=\frac{1}{2}\sum_{\mu}^{N_{TS}}k_{\mu 0}Q_\mu^2+\frac{1}{2}\sum_{\nu}^{N_{NTS}}k_{\nu 0}Q_\nu^2+\ldots \qquad (1)$$

In this expression, the ground state electronic energy at equilibrium is taken as a reference for the energy scale and the equilibrium structure is the reference for the vibrational coordinates. In Eq. 1, the leading terms are quadratic and diagonal, and, for convenience, we have divided the normal modes into N_{TS} totally symmetric, $\{Q_\mu\}$, and N_{NTS} non-totally symmetric, $\{Q_\nu\}$. Then, the energy of an excited electronic state, E_i, can be written as:

$$E_i(Q_1,Q_2,\ldots)=E_{i,e}+\frac{1}{2}\sum_{\mu}^{N_{TS}}k_{\mu i}(Q_\mu-Q_{\mu i})^2+\frac{1}{2}\sum_{\nu}^{N_{NTS}}k_{\nu i}Q_\nu^2+\ldots . \qquad (2)$$

Here, $E_{i,e}$ is the the mininum-to-minimum excitation energy from the ground state (vertical offset), $Q_{\mu i}$ is the vibrational offset of the Q_μ totally symmetric normal mode with the ground state (horizontal offset), and it is clear that non-totally symmetric normal modes have null offsets (because symmetry makes all linear Q_ν terms of the electronic energy to vanish). Eq. 2 implies that non-totally symmetric normal modes only contribute to electronic energy difference if the respective force constants are different, e.g. $k_{\nu 0}\neq k_{\nu i}$. Usually, such contributions are much smaller than those due to vibrational equilibrium offsets. So, the leading term of E_i-E_0 is due to the totally symmetric vibrational modes,

$$E_i(Q_1,Q_2,\ldots)-E_0(Q_1,Q_2,\ldots)=E_{i,e}+\frac{1}{2}\sum_{\mu}^{N_{TS}}k_{\mu i}(Q_\mu-Q_{\mu i})^2-\frac{1}{2}\sum_{\mu}^{N_{TS}}k_{\mu 0}Q_\mu^2+\ldots . \qquad (3)$$

In some highly symmetric active centers, like O_h octahedral ML_6 sites and cubic ML_8 sites, only the breathing modes are totally symmetric. In these cases, if the vibration of the first coordination shell is the only relevant, one single breathing mode contributes in Eq. 3,

$$Q_{\text{breath}}=\frac{1}{\sqrt{n}}\left(\delta_{L_1}+\delta_{L_2}+\ldots+\delta_{L_n}\right), \qquad (4)$$

n being the number of breathing ligands and δ_{L_i} the increment of the M-L_i distance with respect to its value in the reference structure.

In a more general case, it is convenient to define a configuration coordinate. In effect, we can make a rotation (unitary transformation) of the N_{TS} totally symmetric vibrational coordinates into a new set $\{Q_{\mu'}\}$, such that one of the transformed coordinates connects directly the minima of the ground and excited states. Let us call this coordinate Q_{eff}. (We represent in Fig. 1 the original and transformed coordinates in the case of two totally symmetric coordinates Q_1 and Q_2.) Then, E_i and E_0 will have a horizontal offset in this coordinate Q_{eff}, but their offset in all other vibrational coordinates will be zero. Accordingly, only the Q_{eff} vibrational mode contributes to the leading term of the E_i-E_0 energy difference,

$$E_i(Q_1,Q_2,\ldots)-E_0(Q_1,Q_2,\ldots)=E_{i,e}+\frac{1}{2}k_{\text{eff},i}(Q_{\text{eff}}-Q_{\text{eff},i})^2-\frac{1}{2}k_{\text{eff},0}Q_{\text{eff}}^2+\ldots . \qquad (5)$$

Q_{eff} is, then, *the configuration coordinate* of the single ion active center, because it is the only one with horizontal offset and the only one that contributes to the leading term of the electronic energy differences.

[We may remark that this configuration coordinate for the potential energy surfaces of two states (ground and excited) is totally equivalent to the reaction coordinate defined between two minima of the potential energy surface of a chemical reaction (reactants and products). Accordingly, for higher-order approximations to the state energies in Eq. 3, the configuration coordinate is not exactly the straight line connecting the minima, but the curve that connects the lowest energy crossing point between the two surfaces with the two minima, with maximum descendent slope. However, we will assume the quadratic approximation is valid for our purposes.]

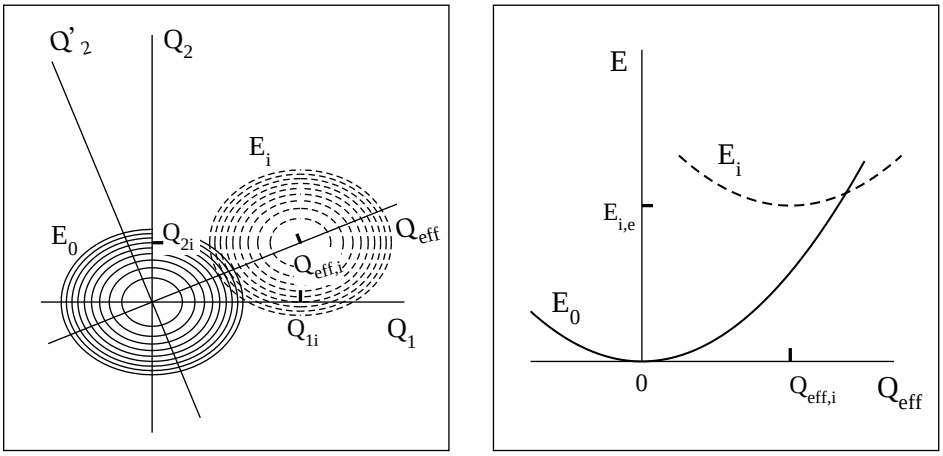

FIG. 1: Left: Definition of the configuration coordinate $Q_{\rm eff}$ of a single ion active center with two totally symmetric normal vibrational modes Q_1 and Q_2. The ground state E_0 and one excited state E_i potential energy surfaces are shown. Right: Corresponding configuration coordinate energy diagram.

We must bear in mind that, in general, the transformed vibrational coordinates are not normal modes, i.e. there are $Q_{\rm eff}Q_{\mu'}$ off-diagonal quadratic terms contributing to the electronic energies. If these terms are negligible, Eq. 5 holds and $Q_{\rm eff}$ is a real vibrational coordinate that connects the minima of E_0 and E_i. Also, if all excited states have their minima alligned with E_0 and E_i in the vibrational space, $Q_{\rm eff}$ is uniquely defined for all states. On the contrary, if $Q_{\rm eff}Q_{\mu'}$ off-diagonal terms are important or the electronic energy minima of all states are far from being alligned, then, for Eq. 5 to hold for all excited states, $Q_{\rm eff}$ must be some sort of not well defined, effective vibrational coordinate. For simplicity, $Q_{\rm eff}$ is often abbreviated by Q. The representation of the energies of the electronic states of the single ion active center along Q is called *the configuration coordinate diagram*.

III. IVCT CONFIGURATION COORDINATE DIAGRAM OF A MIXED VALENCE PAIR

In this Section we describe the configuration coordinate diagram of the intervalence charge transfer (IVCT) states of donor-acceptor dopant pairs in a solid host. We will take an Yb^{2+}/Yb^{3+} mixed valence pair in Yb-doped YAG ($Y_3Al_5O_{12}$) as a working example. We will assume both Yb ions substitute for Y in a D_2 symmetry site with 8-fold Oxygen coordination (with long-range charge compensation in the case of Yb^{2+}) and we will focus on the $4f^N$ manifold. Consequenly, we are interested in the energy levels resulting from the interplay between the $4f^{14}$ electronic configuration of Yb^{2+} and the $4f^{13}$ electronic configuration of Yb^{3+}. The $4f^{14}$ closed-shell configuration of Yb^{2+} has a single totally symmetric A state. As it is shown in Table I, the $4f^{13}$ open-shell configuration of Yb^{3+} has seven Γ_5 Kramers doublets which are grouped into four $^2F_{7/2}$ related levels spanning about 800 cm^{-1} and three $^2F_{5/2}$ related levels spanning about 500 cm^{-1} and lying at about 10000 cm^{-1} above.[14]

TABLE I: Level energies relative to their respective ground states ($E_{i,e}$, in cm^{-1}) and increments of the average Yb-O and Ce-O distances with respect to their values in the ground states of YAG:Yb^{3+} and YAG:Ce^{3+}, respectively (Δd, in Å).

Level	$E_{i,e}$ [a]	Δd [e]	Level	$E_{i,e}$ [b]	Δd [e]
YAG:Yb^{3+}			YAG:Ce^{3+}		
$4f^{13}$ levels			$4f^{1}$ levels		
1 $\Gamma_5(^2F_{7/2})$	0	0	1 $\Gamma_5(^2F_{5/2})$	0	0
2 $\Gamma_5(^2F_{7/2})$	611	0.00	2 $\Gamma_5(^2F_{5/2})$	289	0.00
3 $\Gamma_5(^2F_{7/2})$	696	0.00	3 $\Gamma_5(^2F_{5/2})$	770 [c]	0.00
4 $\Gamma_5(^2F_{7/2})$	782	0.00	4 $\Gamma_5(^2F_{7/2})$	2112	0.00
5 $\Gamma_5(^2F_{5/2})$	10321	0.00	5 $\Gamma_5(^2F_{7/2})$	2342	0.00
6 $\Gamma_5(^2F_{5/2})$	10620	0.00	6 $\Gamma_5(^2F_{7/2})$	2466	0.00
7 $\Gamma_5(^2F_{5/2})$	10674	0.00	7 $\Gamma_5(^2F_{7/2})$	3830	0.00
			Lowest $5d^1$ level		
			8 $\Gamma_5(5d)$	20450 [d]	–0.02
YAG:Yb^{2+}			YAG:Ce^{4+}		
A	0	0.14	A	0	–0.16

[a] Reference 14.
[b] Reference 15.
[c] Reference 16.
[d] Reference 17.
[e] See text.

Let us label the two distinguishable Yb dopant atoms of an Yb^{2+}/Yb^{3+} mixed valence pair as Yb_L and Yb_R. Starting with an Yb_L^{2+}-Yb_R^{3+} ionic configuration of the pair, we have seven levels with the same relative energies of the Yb^{3+} levels. Besides these states, we have those that result from electron transfer from Yb^{2+} to Yb^{3+}. Such electron transfer produces an Yb_L^{3+}-Yb_R^{2+} ionic configuration of the pair,

which also has seven levels with the same relative energies of the Yb^{3+} levels. These are called the IVCT states (of the original, reference Yb_L^{2+}-Yb_R^{3+} pair; obviously, the two sets of seven states are each others' IVCT states.) Altogether, the $4f^N$ manifold of an Yb^{2+}/Yb^{3+} mixed valence pair in YAG is made of 14 energy levels. The energies of the seven levels of the Yb_L^{2+}-Yb_R^{3+} ionic configuration vary with the displacements of the oxygens around Yb_L and Yb_R, but their differences are very insensitive to these displacements because of the $5s^25p^6$ shielding of the $4f$ shells. The same is true for the seven levels of the Yb_L^{3+}-Yb_R^{2+} ionic configuration. On the contrary, the energy differences *between* the two sets of levels are very much dependent on the positions of the oxygens because they involve an ionization in one site and an electron attachement in the complementary site. Here we describe this dependence.

A. IVCT model

In order to facilitate the extension to other mixed valence pairs and to simplify the notation, we well call Yb^{2+} the donor D and Yb^{3+} the acceptor A. More precisely, D and A will not refer to the single Yb ions, but to the defect centers they create in the solid; usually these are atomic moieties containing the Yb ions and their first coordination shells at least. Then the Yb_L^{2+}-Yb_R^{3+} ionic configuration of the Yb^{2+}/Yb^{3+} mixed valence pair can be called D_LA_R, or simply DA, and the Yb_L^{3+}-Yb_R^{2+} ionic configuration A_LD_R, or simply AD.

Let us describe first the energy of the electronic ground state of the Yb^{2+}/Yb^{3+} mixed valence pair as a function of two normal modes Q_L and Q_R, which describe vibrations around Yb_L and Yb_R respectively. We will comment later on the excited states. We may think of Q_L and Q_R as the configuration coordinates (Sec. II) of the Yb_L and Yb_R active centers. In general, they can be any totally symmetric normal vibrational coordinate of the centers.

The adiabatic ground state energy of the Yb^{2+}/Yb^{3+} pair at any value of Q_L and Q_R can be seen as the result of the diagonalization of a 2×2 Hermitean matrix whose diagonal elements are the energies of the Yb_L^{2+}-Yb_R^{3+} and Yb_L^{3+}-Yb_R^{2+} ionic configurations of the pair (diabatic energies $H_{11}=E_{D_0A_0}$ and $H_{22}=E_{A_0D_0}$), and with the electronic coupling between the two ionic configurations as the off-diagonal element H_{12}. This diagonalization also gives the adiabatic energy of a second, excited state at each Q_L and Q_R. The consideration of the H_{12} electronic coupling is central for the energy barrier of the thermal electron transfer reaction Yb_L^{2+}-Yb_R^{3+} → Yb_L^{3+}-Yb_R^{2+} and for the radiative and non-radiative transition probabilities. However, it is of minor importance for the energy of the corresponding optical electron transfer, which takes place at a fixed equilibrium structure of Yb_L^{2+}-Yb_R^{3+} with a relatively long Yb-Yb distance, and for the values of the vibrational coordinates at which crossings between potential energy surfaces occur.[9,10] In consequence, we will discuss the diabatic energies of Yb_L^{2+}-Yb_R^{3+} and Yb_L^{3+}-Yb_R^{2+}, which correspond to null electronic coupling between the oxidized and reduced members of the pair.

The diabatic energy of the ground state of the DA ionic configuration, as a function of the positions of the ligands that can be described with the coordinates Q_L and Q_R, can be written as

$$E_{D_0A_0}(Q_L,Q_R)=\frac{1}{2}k(Q_L-Q_{D_0})^2+\frac{1}{2}k(Q_R-Q_{A_0})^2\,, \quad (6)$$

in a quadratic approximation with a common force constant for D and A, $k=\mu\omega^2$, μ being the reduced mass of the vibration and ω the vibrational frequency common to both vibrational coordinates. This equation establishes the minimum of $E_{D_0A_0}$ as the reference energy. Q_{D_0} and Q_{A_0} are the values of the vibrational coordinates at the equilibrium structures of D and A respectively. Equivalently, if the donor and acceptor sites are identical, the diabatic energy of the ground state of the AD ionic configuration is

$$E_{A_0D_0}(Q_L,Q_R)=\frac{1}{2}k(Q_L-Q_{A_0})^2+\frac{1}{2}k(Q_R-Q_{D_0})^2\,. \quad (7)$$

The diabatic potential energy surface $E_{A_0D_0}(Q_L,Q_R)$ is identical to $E_{D_0A_0}(Q_L,Q_R)$ but shifted $-(Q_{D_0}-Q_{A_0})$ in the Q_L axis and $+(Q_{D_0}-Q_{A_0})$ in the Q_R axis. They are represented in Fig 2.

The crossing point between $E_{D_0A_0}$ and $E_{A_0D_0}$ with lowest energy is the activated complex (ac) of the thermal $DA\rightarrow AD$ electron transfer reaction at the diabatic level. Within the adopted approximations of identical D and A sites and a common force constant for both, this activated complex is at the midpoint between their respective minima: $Q_{L,ac}=Q_{R,ac}=Q_{ac}\equiv(Q_{D_0}+Q_{A_0})/2$. The electron transfer reaction coordinate is the straight line in the (Q_L,Q_R) plane that connects the $E_{D_0A_0}$ and $E_{A_0D_0}$ minima and passes through the activated complex,

$$\frac{Q_L-Q_{D_0}}{Q_R-Q_{A_0}}=-1\,. \quad (8)$$

Then, a normal electron transfer reaction coordinate Q_{et} can be defined,

$$Q_{et}=\frac{1}{\sqrt{2}}(Q_R-Q_L)\,, \quad (9)$$

which is null for the activated complex, $Q_{et,ac}$=0, and takes opposite values for the DA and AD ionic configurations at the equilibrium,

$$-Q_{et,D_0A_0}=Q_{et,A_0D_0}=\frac{1}{\sqrt{2}}(Q_{D_0}-Q_{A_0})\,, \quad (10)$$

which gives

$$Q_{et,A_0D_0}-Q_{et,D_0A_0}=\sqrt{2}(Q_{D_0}-Q_{A_0})\,. \quad (11)$$

Using the Q_{et} defined in Eq. 9, the parametric form of the reaction coordinate is

$$\begin{cases} Q_L-Q_{ac}=-\dfrac{1}{\sqrt{2}}Q_{et}\,,\\ Q_R-Q_{ac}=+\dfrac{1}{\sqrt{2}}Q_{et}\,, \end{cases} \quad (12)$$

which makes it clear that an increment of Q_{et} means a simultaneous decrement of Q_L and increment of Q_R. This reflects the fact that a thermal electron transfer from D_L to A_R, which converts $D_L A_R$ into $A_L D_R$, is accompanied by a contraction of the coordination shells around the donor D_L and a simultaneous expansion around the acceptor A_R.

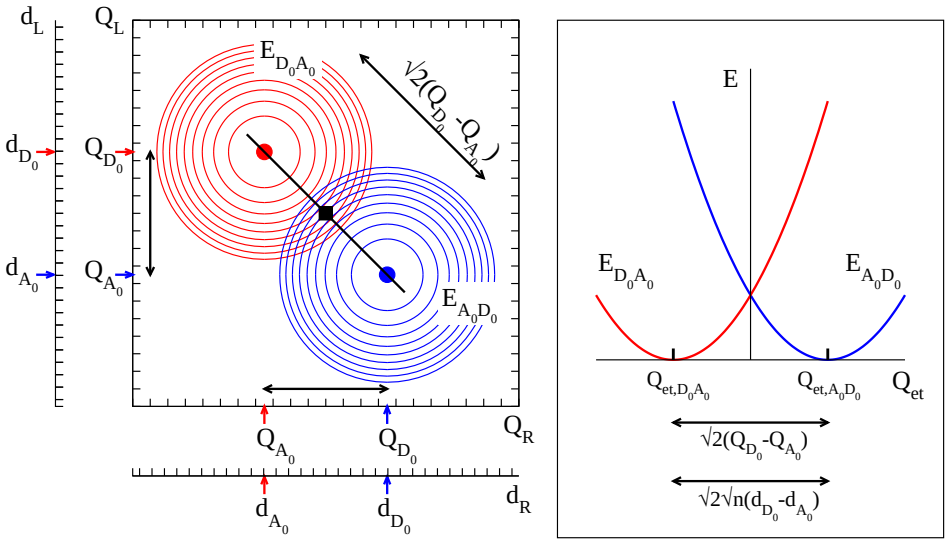

FIG. 2: Left: Ground state diabatic energy surfaces of the *DA* (red) and *AD* (blue) ionic configurations of the mixed valence pair. The black line that connects the *DA* minimum (red dot) with the *AD* minimum (blue dot) and passes trhough the activated complex (black square) is the electron transfer reaction coordinate, which is also the IVCT configuration coordinate. Right: IVCT configuration coordinate diagram with the ground state energies of *DA* (red) and *AD* (blue).

Accordingly, the energies of the two ionic configurations of the Yb^{2+}/Yb^{3+} mixed valence pair along the reaction coordinate are:

$$E_{D_0A_0}(Q_{et}) = \frac{1}{2}k(Q_{et} - Q_{et,D_0A_0})^2\,,$$
$$E_{A_0D_0}(Q_{et}) = \frac{1}{2}k(Q_{et} - Q_{et,A_0D_0})^2\,, \qquad (13)$$

which are two identical parabolae with a horizontal offset $\sqrt{2}(Q_{D_0} - Q_{A_0})$,

$$E_{D_0A_0}\left(Q_{et} - \sqrt{2}(Q_{D_0} - Q_{A_0})\right) = E_{A_0D_0}\left(Q_{et}\right)\,. \qquad (14)$$

Since the coordinate orthogonal to Q_{et} does not have a horizontal offset (Fig. 2), the reaction coordinate Q_{et} is the IVCT configuration coordinate. The horizontal offset and the force constant k are the only two degrees of freedom of this model.

If Q_L and Q_R are the respective breathing modes of the Yb_L and Yb_R substitutional defects in YAG, which normaly produce the maximum energy changes, they can be written as

$$Q_L = \frac{1}{\sqrt{8}}\left(\delta_{O_{L1}} + \delta_{O_{L2}} + \ldots + \delta_{O_{L8}}\right)\,,$$
$$Q_R = \frac{1}{\sqrt{8}}\left(\delta_{O_{R1}} + \delta_{O_{R2}} + \ldots + \delta_{O_{R8}}\right)\,, \qquad (15)$$

$\delta_{O_{L1}}$ being the increment of the Yb_L-O_{L1} distance with respect to its value in a given reference structure, and equivalently for the displacements of the other oxygens. The electron transfer reaction coordinate Q_{et} defined in Eq. 9 that corresponds to these definitions of Q_L and Q_R are shown in Fig. 3. Since all the Yb-O distances change equally during the breathing, we can write

$$Q_L = \sqrt{8}\,(d_L - d_{\text{ref}})\,,\ \ Q_R = \sqrt{8}\,(d_R - d_{\text{ref}})\,, \qquad (16)$$

where d_{ref}, d_L, and d_R are, respectively, the average Yb-O distances in a reference structure, and around Yb_L and Yb_R at any moment. Then, for the donor and acceptor equilibrium structures we have

$$Q_{D_0} = \sqrt{8}\left(d_{D_0} - d_{\text{ref}}\right)\,,\ \ Q_{A_0} = \sqrt{8}\left(d_{A_0} - d_{\text{ref}}\right)\,, \qquad (17)$$

d_{D_0} and d_{A_0} being the average Yb-O distances around the donor Yb^{2+} and the acceptor Yb^{3+} at equilibrium. In a more general case with a coordination number n of equal ligands,

$$Q_{D_0} = \sqrt{n}\left(d_{D_0} - d_{\text{ref}}\right)\,,\ \ Q_{A_0} = \sqrt{n}\left(d_{A_0} - d_{\text{ref}}\right)\,. \qquad (18)$$

This leads to the centers of the two parabolae in the configuration coordinate diagram (Eq. 13),

$$-Q_{et,D_0A_0} = Q_{et,A_0D_0} = \sqrt{n/2}(d_{D_0} - d_{A_0})\,, \qquad (19)$$

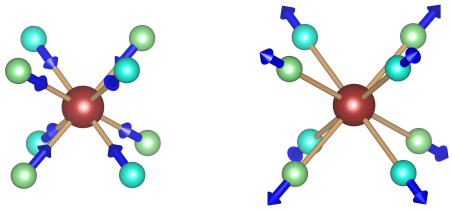

FIG. 3: Electron transfer reaction coordinate Q_{et} of an Yb^{2+}/Yb^{3+} pair in YAG.

and their offset

$$\sqrt{2}(Q_{D_0} - Q_{A_0}) = \sqrt{2n}\left(d_{D_0} - d_{A_0}\right). \qquad (20)$$

Then, the horizontal offset (which is key to the model, together with the force constant) can be estimated from the difference between the ionic radii of the donor and acceptor ions, Yb^{2+} and Yb^{3+} in our working example.

The diabatic potential energy surfaces of other states of the $4f^N$ manifold of the Yb^{2+}/Yb^{3+} mixed valence pair can be written as

$$\begin{aligned} E_{D_iA_j}(Q_L,Q_R) &= E_{D_iA_j,e} + \frac{1}{2}k(Q_L - Q_{D_0})^2 \\ &\quad + \frac{1}{2}k(Q_R - Q_{A_0})^2 \\ E_{A_jD_i}(Q_L,Q_R) &= E_{D_iA_j,e} + \frac{1}{2}k(Q_L - Q_{A_0})^2 \\ &\quad + \frac{1}{2}k(Q_R - Q_{D_0})^2, \end{aligned} \qquad (21)$$

assuming they have the same equilibrium structures and vibrational frequencies as the ground state. The vertical offsets $E_{D_iA_j,e}$ are the sum of the minimum-to-minimum excitation energies from the ground state to the i excited state of D and from the ground state to the j excited state of A: $E_{D_iA_j,e} = (E_{D_i,e} - E_{D_0,e}) + (E_{A_j,e} - E_{A_0,e})$. Those of the two complementary states D_iA_j and A_jD_i are identical: Then, their energies in the IVCT configuration coordinate diagram are

$$\begin{aligned} E_{D_iA_j}(Q_{et}) &= E_{D_iA_j,e} + \frac{1}{2}k(Q_{et} - Q_{et,D_0A_0})^2, \\ E_{A_jD_i}(Q_{et}) &= E_{D_iA_j,e} + \frac{1}{2}k(Q_{et} - Q_{et,A_0D_0})^2. \end{aligned} \qquad (22)$$

In summary, Eq. 22, together with Eq. 19, or in a more general case with Eq. 10, constitute an IVCT configuration coordinate (diabatic) diagram of the D/A mixed valence pair.

The model of the potential energy surfaces can be improved by extending Eq. 21. Using different force constants for D and A leads to a different electron transfer reaction cooordinate but a configuration coordinate diagram like Eq. 22 can still be used.[9] In this case, the minima of DA and AD are not alligned with the activated complex and the reaction coordinate is made of two straight segments, one between DA and the activated complex and another between the activated complex and AD. Also, using state-specific equilibrium structures, or state-specific force constants, or including anharmonic terms, will prevent from defining a unique reaction coordinate, because there is a different one for each D_iA_j-A_kD_ℓ combination. In the case of excited states of a different configuration, like $4f^{N-1}5d$, using state-specific equilibrium structures, or at least configuration-specific equilibrium structures, might be neccesary. If so, the one-dimension configuration coordinate diagram will break in a strict sense and working with the two-dimension energy surfaces is compulsory. However, the reaction coordinates of several D_iA_j-A_kD_ℓ combinations can be similar enough so as to make the representation of all states of the mixed valence pair along one of these reaction coordinates meaningful.[9]

B. IVCT configuration coordinate diagram of Yb^{2+}/Yb^{3+} in YAG

In Fig. 4 we show the IVCT configuration coordinate diagram of the $4f^N$ levels of an Yb^{2+}/Yb^{3+} mixed valence pair in YAG. It results from using Eqs. 19 and 22 with n=8 and the following data: (1) The $E_{D_iA_j,e}$ are the experimental $4f \rightarrow 4f$ excitation energies of Yb^{3+}, which are shown in the second column of Table I (note that Yb^{2+} has only one state of the $4f^{14}$ configuration). (2) For the $d_{D_0} - d_{A_0}$ offset between donor and acceptor equilibrium distances, which is $d_{Yb^{2+}-O} - d_{Yb^{3+}-O}$, we have taken 90% of the difference between the ionic radii of Yb^{2+} and Yb^{3+} in coordination 8 (1.14 Å and 0.985 Å respectively, Ref. 18), which is $d_{D_0} - d_{A_0}$= 0.14 Å. The reduction factor has been used to take into accound the host effect, which has been found to make the equilibrium impurity-ligand distance in a doped host to lie between the cation-ligand distance in the undoped host and the distance that would correspond to the ionic radii mismatch between the host cation and the impurity.[19] (3) The force constant is $k = \mu\omega^2$, with μ=m(O)=15.999 amu. We are not aware of direct experimental determinations of the breathing mode vibrational frequency of Yb^{3+} defects in YAG; we have taken a $\bar{\nu} = \omega/(2\pi c)$=326 cm^{-1} mode reported by Lupei *et al.*[20] after an analysis of resonant vibronic effects in YAG:Yb^{3+} and have scaled it 0.95% down to 310 cm^{-1}. This corresponds to a 90% scaling of the force constant k, which is expected to be smaller in Yb^{2+} than in Yb^{3+}. Since

$$\frac{k}{\mathrm{cm^{-1}\,\AA^{-2}}} = 0.029660 \times \left(\frac{\mu}{\mathrm{amu}}\right) \times \left(\frac{\bar{\nu}}{\mathrm{cm^{-1}}}\right)^2,$$

we get k = 50434 cm^{-1} Å^{-2}.

In the IVCT configuration coordinate diagram (Fig. 4) we observe the energies of the seven levels of the Yb_L^{2+}-Yb_R^{3+} (in red) and the seven levels of the Yb_L^{3+}-Yb_R^{2+} (in blue) ionic configurations of the pair. They are grouped in two sets of

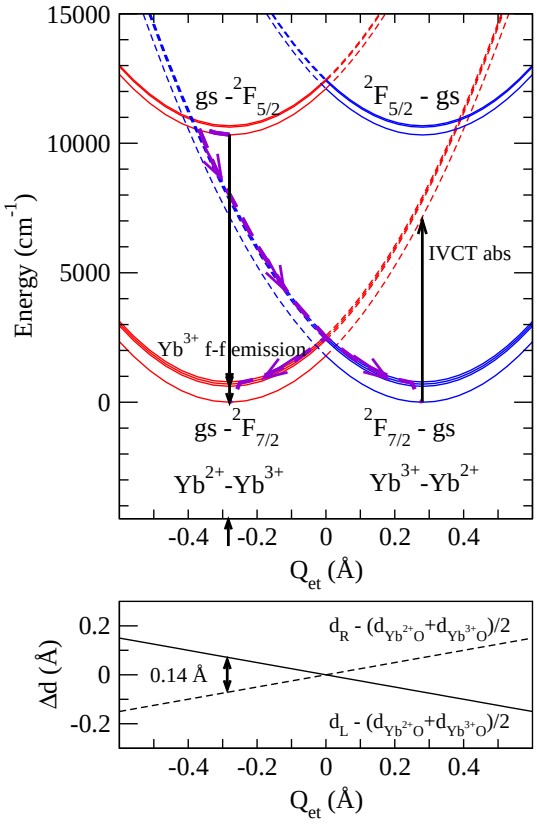

FIG. 4: Top: IVCT configuration coordiante diagram of a Yb^{2+}/Yb^{3+} mixed valence pair in YAG. Bottom: Changes of the Yb-O distance in the left Yb (d_L, full line) and right Yb (d_R, dashed line) with respect to their value at the activated complex, $(d_{Yb^{2+}-O,e}+d_{Yb^{3+}-O,e})/2$, along the configuration coordinate (or electron transfer reaction coordinate) Q_{et}.

four levels corresponding to $Yb_R^{3+}(^2F_{7/2})$ and $Yb_L^{3+}(^2F_{7/2})$, and two sets of three levels about 10000 cm^{-1} above, corresponding to $Yb_R^{3+}(^2F_{5/2})$ and $Yb_L^{3+}(^2F_{5/2})$. They have been represented with full lines for configuration coordinate values around their respective minima. We used dashes lines for their energies at configuration coordinate values corresponding to stressed structures. For instance, at Q_{et}=–0.28 Å we find Yb_L^{2+}-Yb_R^{3+} in equilibrium (full lines), with a long Yb_L-O distance and a short Yb_R-O distance; on the contrary, an Yb_L^{3+}-Yb_R^{2+} state is under strong stress in such structure (dashed lines) and it will relax towards a short Yb_L-O distance and a long Yb_R-O distance, increasing Q_{et} and releasing a large reorganization energy (about 7500 cm^{-1}). It is clear that structurally stressed IVCT states intercalate between states of the pairs around their equilibrium. Vertical (Frank-Condon) transitions between full lines take place in Yb^{3+}. Vertical transitions between full and dashed lines are IVCT transitions; they end in structurally stressed states and take place between states with large horizontal offsets, which produces very wide bands. IVCT absorptions in mixed valence compounds are known long ago;[5,6] they take place without a corresponding emission. IVCT emissions from higher excited states have been recently reported in mixed valence dopant pairs in solids. They have been found to be responsible for the anomalous emission of Ce^{3+}-doped elpasolites[9] and for the interplay between anomalous emissions and $5d \rightarrow 4f$ emissions in Yb-doped fluorite hosts.[10] The IVCT emissions have large Stokes shifts associated with large reorganization energies.

It is interesting to observe in the IVCT configuration coordinate diagram that IVCT crossings between the excited Yb_L^{2+}-$Yb_R^{3+}(^2F_{5/2})$ and the ground $Yb_L^{3+}(^2F_{7/2})$-Yb_R^{2+} manifolds can occur with low energy barriers. Obviously, the same is true for their symmetrical counterparts. With the present data we obtain a 200 cm^{-1} energy barrier from the minimum of the Yb_L^{2+}-$Yb_R^{3+}(^2F_{5/2})$ state (which is the emitting state of the Yb^{3+} $4f \rightarrow 4f$ emission) to the crossing between the lowest Yb_L^{2+}-$Yb_R^{3+}(^2F_{5/2})$ level and the highest $Yb_L^{3+}(^2F_{7/2})$-Yb_R^{2+} level. This result suggests the consideration of the nonradiative $Yb^{2+}(4f_{7/2}) \rightarrow Yb^{3+}(4f_{5/2})$ electron transfer in Yb^{2+}/Yb^{3+} pairs as a possible mechanism responsible for quenchings of the Yb^{3+} emission, which is shown in violet in Fig. 4. This means that Yb^{2+}/Yb^{3+} pairs can be the active quenchers in the concentration quenching of the Yb^{3+} emission.[21] Also, they can explain the temperature quenching of the Yb^{3+} emission excited with Ce^{3+} $4f \rightarrow 5d$ absorption in Ce,Yb-codoped YAG.[3]

The uncertainities of the empirical data used to build the configuration coordinate diagram in Fig. 4 give only a qualitative or semi-quantiative meaning to the energy barrier just discussed. For instance, taking 95% or 85% of the ionic radii difference for $d_{Yb^{2+}-O} - d_{Yb^{3+}-O}$ instead of 90%, leads to 75 cm^{-1} and 400 cm^{-1} energy barriers instead of the 200 cm^{-1} mentioned above. Similarly, using a higher/lower vibrational frequency would decrease/increase the barrier value in this case. Besides, the effective activation energies that are experimentally determined are smaller than the barrier energies calculated from configuration coordinate diagrams because of the effective overlap between vibrational wavefunctions below the crossing points.[22] Nevertheless, it is clear that a configuration coordinate diagram obtained with reasonable empirical data indicates that a crossing between a potentially emitting level Yb_L^{2+}-$Yb_R^{3+}(^2F_{5/2})$ and a structurally stressed IVCT ground state level $Yb_L^{3+}(^2F_{7/2})$-Yb_R^{2+} is likely to occur and it would cause thermal quenching of the Yb^{3+} $4f \rightarrow 4f$ emission.

IV. MMCT CONFIGURATION COORDINATE DIAGRAM OF A METAL-METAL PAIR

In this Section, we describe the configuration coordinate diagram of the metal-to-metal charge transfer states of a pair of ions of different elements in a solid host. We will take a Ce^{3+}-Yb^{3+} pair in Ce,Yb-codoped YAG as a working example. We assume Ce^{3+} and Yb^{3+} substitute for Y in a D_2 symmetry site with 8-fold Oxygen coordination. Regarding Ce^{3+}, we will focus on its states of the $4f^1$ configuration and on its lowest $5d^1$ state. As

it is shown in Table I, the seven $4f^1$ states are grouped in three sets:[15,16] a first set with three levels spanning about 800 cm^{-1}, 1-3 Γ_5; a second set starting at about 2100 cm^{-1} above the ground sate with three levels spanning 350 cm^{-1}, 4-6 Γ_5; and a third set at about 3800 cm^{-1} above the ground state with one level, 7 Γ_5. (This distribution of levels differs from the extended assumption of three $^2F_{5/2}$ related levels and four $^2F_{7/2}$ related levels separated by about 2500 cm^{-1}; a $4f$ crystal field splitting of the same size of the $4f$ spin-orbit coupling splitting is responsible for the partial break of such assumption.[16]) The lowest $5d^1$ state is 20450 cm^{-1} above the ground state.[17] These levels will combine with the previously described four $^2F_{7/2}$ related levels and three $^2F_{5/2}$ related levels of Yb^{3+} (Sec. III). The result of this combination is four main sets of levels. A first main set of 28 levels of $Ce^{3+}(4f^1)$-$Yb^{3+}(^2F_{7/2})$ character lies between 0 and 4600 cm^{-1} and is divided in three subsets: 12 Ce^{3+}(1-3 Γ_5)-$Yb^{3+}(^2F_{7/2})$, 12 Ce^{3+}(4-6 Γ_5)-$Yb^{3+}(^2F_{7/2})$, and 4 Ce^{3+}(7 Γ_5)-$Yb^{3+}(^2F_{7/2})$. A second main set of 21 levels of $Ce^{3+}(4f^1)$-$Yb^{3+}(^2F_{5/2})$ character lies between 10300 cm^{-1} and 14500 cm^{-1} and is divided in three subsets: 9 Ce^{3+}(1-3 Γ_5)-$Yb^{3+}(^2F_{5/2})$, 9 Ce^{3+}(4-6 Γ_5)-$Yb^{3+}(^2F_{5/2})$, and 3 Ce^{3+}(7 Γ_5)-$Yb^{3+}(^2F_{5/2})$. A third main set of 4 levels of $Ce^{3+}(5d_1^1)$-$Yb^{3+}(^2F_{7/2})$ character lies between 20450 cm^{-1} and 21230 cm^{-1}. Finally a fourth main set of 4 levels of $Ce^{3+}(5d_1^1)$-$Yb^{3+}(^2F_{5/2})$ character lies between 30770 cm^{-1} and 31120 cm^{-1}. Between the third and the fourth set, states of $Ce^{3+}(5d_2^1)$-$Yb^{3+}(^2F_{7/2})$ character associated with the second $5d^1$ excited state of Ce^{3+} may appear. Here we will only pay attention to the three first sets.

Electron transfer from Ce^{3+} to Yb^{3+} results into a Ce^{4+}-Yb^{2+} pair with a closed-shell ground state much more stable than all its excited states. This level may lie between the Ce^{3+}-Yb^{3+} states just discussed. Such a consideration has led to propose its involvement in the mechanism of energy transfer from Ce^{3+} to Yb^{3+} in Ce,Yb-codoped YAG, as well as in the quenching of the Ce^{3+}-excited Yb^{3+}-emission of this material.[3] The question we tackle here is how to represent the energies of the levels of the Ce^{3+}-Yb^{3+} and Ce^{4+}-Yb^{2+} pairs together in a simplified diagram, which is called the MMCT configuration coordinate diagram.

A. MMCT model

In order to make the notation more general, we will call Ce^{3+} the donor D and Yb^{3+} the acceptor A. After the electron transfer they result into Ce^{4+} and Yb^{2+}, which will be respectively called D^+ and A^-. As in the IVCT case, D, A, D^+, and A^- refer to the defect centers the respective ions create in the solid, which will be atomic moieties containing at least their first coordination shells, rather than to the single ions. Then, the pair Ce^{3+}-Yb^{3+} is DA and the pair Ce^{4+}-Yb^{2+} is D^+A^-.

We aim at describing the energies of the states of the Ce^{3+}-Yb^{3+} and Ce^{4+}-Yb^{2+} pairs (DA and D^+A^-) as functions of two vibrational coordinates Q_D and Q_A, which describe vibrations of the moieties containing Ce (D and D^+) and Yb (A and A^-) respectively. Note that in MMCT, contrary to IVCT, D and D^+ refer to a different element than A and A^-, so that there is no need to use the *left* and *right* atoms to differentiate them; in other words, Ce is always the *left* atom and Yb the *right* atom. This is why we use Q_D and Q_A here instead of Q_L and Q_R. As in IVCT, Q_D and Q_A can be the configuration coordinate described in Sec. II of the Ce and Yb active centers, but they can also be other totally symmetric vibrational coordinates of these centers.

The diabatic energy of the ground state of the DA pair, as a function of the positions of the ligands that can be described with the coordinates Q_D and Q_A, can be written as

$$E_{D_0A_0}(Q_D,Q_A) = \frac{1}{2}k_D(Q_D-Q_{D_0})^2 + \frac{1}{2}k_A(Q_A-Q_{A_0})^2\,, \qquad (23)$$

in a quadratic approximation. Q_{D_0} and Q_{A_0} are the values of the vibrational coordinates of the donor and acceptor moieties at the respective equilibrium structures of D and A. $k_D = \mu_D\omega_D^2$ and $k_A = \mu_A\omega_A^2$ are, respectively, the donor and acceptor force constants, μ_D and μ_A their vibrational masses, and ω_D and ω_A their vibrational frequencies. As in IVCT, with this equation we are establishing the ground state energy of the DA pair at its minimum as the reference energy.

The diabatic energy of the ground state of the D^+A^- pair that results after MMCT from DA can be written as

$$E_{D_0^+A_0^-}(Q_D,Q_A) = E_{D_0^+A_0^-,e} + \frac{1}{2}k_D(Q_D-Q_{D_0^+})^2 + \frac{1}{2}k_A(Q_A-Q_{A_0^-})^2\,. \qquad (24)$$

Here, as in the IVCT model of Sec. III, we assume a common force constant k_D for D and D^+ on one side, and k_A for A and A^- on the other; $Q_{D_0^+}$ and $Q_{A_0^-}$ are the values of the vibrational coordinates of the donor and acceptor moieties at the respective equilibrium structures of D^+ and A^-. $E_{D_0^+A_0^-,e}$ is the vertical offset between the minima of the D^+A^- and DA ground state potential energy surfaces. In an empirical approach to the problem, it can be considered an empirical parameter. Also, it might eventually be convinent to regard it as the sum of: 1) the adiabatic ionization potential of D in the host, IP_D (energy difference between the ground states of D^+ and D at their relaxed structures), 2) the negative adiabatic electron affinity of A in the host, $-EA_A$ (energy difference between the ground states of A^- and A at their relaxed structures), and 3) the interaction energy change due to the creation of a hole in D and an electron in A; for long D-A separations, this can be approximated by $(q_A-q_D-1)/d_{DA}$, d_{DA} being the distance between donor and acceptor, and q_D and q_A their respective charges:

$$E_{D_0^+A_0^-,e} = IP_D - EA_A + (q_A-q_D-1)/d_{DA}\,. \qquad (25)$$

The $E_{D_0A_0}(Q_D,Q_A)$ and $E_{D_0^+A_0^-}(Q_D,Q_A)$ potential energy surfaces are represented in the left hand side of Fig. 5.

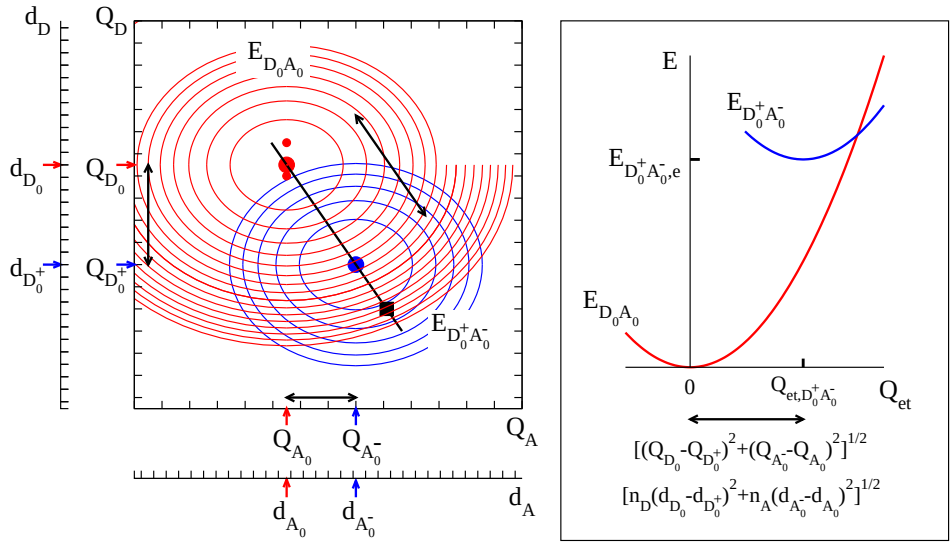

FIG. 5: Left: Ground state diabatic energy surfaces of DA (red) and D^+A^- (blue). The black line that connects the DA minimum (red dot) with the activated complex (black square) and returns to the D^+A^- minimum (blue dot) is the electron transfer reaction coordinate, which is also the MMCT configuration coordinate. The minima of other two DA energy surfaces (not represented here) are indicated with red dots. Right: MMCT configuration coordinate diagram with the ground state energies of DA (red) and D^+A^- (blue).

Within these approximations, the activated complex of the thermal $DA \rightarrow D^+A^-$ reaction is in the straight line that connects their minima. Its exact position depends on the value of the energy offset $E_{D_0^+A_0^-,e}$. In any case, as in the IVCT case, the electron transfer reaction coordinate is the straight line in the (Q_D,Q_A) plane that passes through the $E_{D_0A_0}$ and $E_{D_0^+A_0^-}$ minima,

$$\frac{Q_D - Q_{D_0}}{Q_A - Q_{A_0}} = m \equiv \frac{Q_{D_0^+} - Q_{D_0}}{Q_{A_0^-} - Q_{A_0}}. \qquad (26)$$

with a negative slope m. Then, a normal reaction coordinate could be defined like in Eq. 9, which would be null in the activated complex. However, since the position of the activated complex can be very different for different pairs of DA and D^+A^- states, it can be more convenient to define here the normal reaction coordinate so that it is null for the DA ground state at equlilbrium:

$$Q_{et} = \frac{1}{\sqrt{1+m^2}}\left[(Q_A - Q_{A_0}) + m(Q_D - Q_{D_0})\right]. \qquad (27)$$

Then, the parametric form of the reaction coordinate is

$$\begin{cases} Q_D - Q_{D_0} = \dfrac{m}{\sqrt{1+m^2}} Q_{et}\,, \\ Q_A - Q_{A_0} = \dfrac{1}{\sqrt{1+m^2}} Q_{et}\,. \end{cases} \qquad (28)$$

which, with a negative m, indicates that an increment of Q_{et} means a simultaneous decrement of Q_D and increment of Q_A.

Being the only coordinate with horizontal offset, Q_{et} is the MMCT configuration coordinate and the energies of the ground states of the Ce^{3+}-Yb^{3+} and Ce^{4+}-Yb^{2+} pairs as functions of it constitute the configuration coordinate diagram for these states. Using Eqs. 23, 24, and 28, they are:

$$\begin{aligned} E_{D_0A_0}(Q_{et}) &= \frac{1}{2}k_{et}(Q_{et} - Q_{et,D_0A_0})^2 \\ E_{D_0^+A_0^-}(Q_{et}) &= E_{D_0^+A_0^-,e} + \frac{1}{2}k_{et}(Q_{et} - Q_{et,D_0^+A_0^-})^2, \end{aligned} \qquad (29)$$

with

$$\begin{aligned} Q_{et,D_0A_0} &= 0 \\ Q_{et,D_0^+A_0^-} &= \sqrt{(Q_{D_0} - Q_{D_0^+})^2 + (Q_{A_0^-} - Q_{A_0})^2}, \end{aligned} \qquad (30)$$

and

$$k_{et} = \frac{1}{1+m^2}(m^2 k_D + k_A). \qquad (31)$$

The MMCT configuration coordinate diagram with $E_{D_0A_0}(Q_{et})$ and $E_{D_0^+A_0^-}(Q_{et})$ is represented in the right hand side of Fig. 5. The three degrees of freedom of this MMCT configuration coordinate diagram are the electron transfer reaction coordinate curvature, k_{et}, the MMCT horizontal offset $\sqrt{(Q_{D_0} - Q_{D_0^+})^2 + (Q_{A_0^-} - Q_{A_0})^2}$, and the vertical offset $E_{D_0^+A_0^-,e}$.

If Q_D and Q_A are the breathing modes of the donor and acceptor, with n_D and n_A equal ligands respectively, we have

$$\begin{aligned} Q_{D_0} - Q_{D_0^+} &= \sqrt{n_D}(d_{D_0} - d_{D_0^+}), \\ Q_{A_0^-} - Q_{A_0} &= \sqrt{n_A}(d_{A_0^-} - d_{A_0}), \end{aligned} \qquad (32)$$

and a horizontal offset

$$Q_{et,D_0^+A_0^-} - Q_{et,D_0A_0} = Q_{et,D_0^+A_0^-} = \sqrt{n_D(d_{D_0} - d_{D_0^+})^2 + n_A(d_{A_0^-} - d_{A_0})^2}\,. \quad (33)$$

For excited states of DA and D^+A^-, the diabatic energy surfaces are

$$\begin{aligned} E_{D_iA_j}(Q_D, Q_A) &= E_{D_iA_j,e} + \frac{1}{2}k_D(Q_D - Q_{D_i})^2 \\ &\quad + \frac{1}{2}k_A(Q_A - Q_{A_j})^2\,, \\ E_{D_k^+A_\ell^-}(Q_D, Q_A) &= E_{D_k^+A_\ell^-,e} + \frac{1}{2}k_D(Q_D - Q_{D_k^+})^2 \\ &\quad + \frac{1}{2}k_A(Q_A - Q_{A_\ell^-})^2\,. \end{aligned} \quad (34)$$

The energy offsets of DA are the sums of the minimum-to-minimum excitation energies from the ground state to the i excited state of D and from the ground state to the j excited state of A: $E_{D_iA_j,e} = (E_{D_i,e} - E_{D_0,e}) + (E_{A_j,e} - E_{A_0,e})$. Correspondingly, the energy offsets of D^+A^- are the sums of the minimum-to-minimum excitation energies from the ground state to the k excited state of D^+ and from the ground state to the ℓ excited state of A^-, plus the ground state energy offset $E_{D_0^+A_0^-,e}$, which fulfils Eq. 25: $E_{D_k^+A_\ell^-,e} = E_{D_0^+A_0^-,e} + (E_{D_k^+,e} - E_{D_0^+,e}) + (E_{A_\ell^-,e} - E_{A_0^-,e})$. The D^+A^- ground state energy offset $E_{D_0^+A_0^-,e}$ is the only parameter of the model that depends on the donor-acceptor distance d_{DA}. This means that, when two or more DA pairs made of the same elements coexist in the same host with different D-A distances, d_{DA} and d'_{DA}, their MMCT manifolds $E_{D_k^+A_\ell^-}$ are identical and shifted in energy with respect to one another. Eq. 25 gives $1/d_{DA} - 1/d'_{DA}$ for the shift.

In general, there will be one reaction coordinate for each D_iA_j-$D_k^+A_\ell^-$ combination. However, if the horizontal offsets between different states of DA is much smaller than the MMCT horizontal offset, it is not a bad approximation to use the ground state reaction coordinate Eq. 27 for all the states. In this case, we have

$$\begin{aligned} E_{D_iA_j}(Q_{et}) &= E_{D_iA_j,e} + \frac{1}{2}k_{et}(Q_{et} - Q_{et,D_0A_0})^2 \\ E_{D_k^+A_\ell^-}(Q_{et}) &= E_{D_k^+A_\ell^-,e} + \frac{1}{2}k_{et}(Q_{et} - Q_{et,D_0^+A_0^-})^2\,. \end{aligned} \quad (35)$$

Summarizing, Eq. 35, together with Eq. 33, or in a more general case with Eq. 30, constitute the MMCT configuration coordinate (diabatic) diagram of the DA and D^+A^- metal-metal pairs in a host.

Alternatively, if the horizontal offsets between different states of either DA or D^+A^- are taken into account, then the MMCT configuration coordinate diagram results from evaluating Eq. 34 along the reaction coordinate of Eqs. 26, 27, and 32. If the reaction coordinate of a set of excited states D_iA_j-$D_k^+A_\ell^-$ is taken as the configuration coordinate, instead of the ground state combination D_0A_0-$D_0^+A_0^-$, then, Eqs. 26 and 27 are still valid to define such a coordinate, as long as Q_{D_0}, Q_{A_0}, $Q_{D_0^+}$, and $Q_{A_0^-}$, are substituted by the corresponding Q_{D_i}, Q_{A_j}, $Q_{D_k^+}$, and $Q_{A_\ell^-}$.

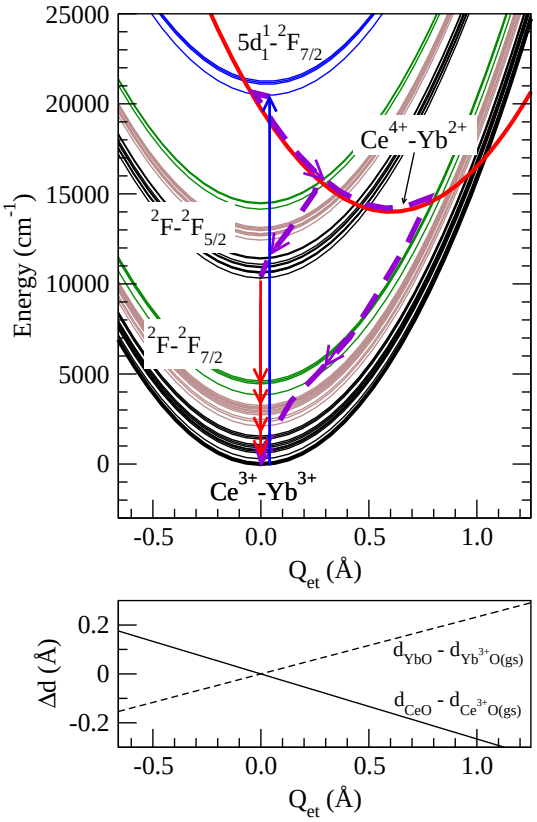

FIG. 6: MMCT configuration coordiante diagram of Ce^{3+}/Yb^{3+} pairs in YAG. The following processes are indicated: Ce^{3+} lowest $4f \rightarrow 5d$ absorption (blue arrow); energy transfer to the $^2F_{5/2}$ excited state of Yb^{3+} and non-radiative decay to the ground states of Ce^{3+} and Yb^{3+} trhough the Ce^{4+}-Yb^{2+} MMCT state (dashed violet line); and Yb^{3+} $4f \rightarrow 4f$ emission (red arrows).

B. MMCT configuration coordinate diagram of Ce^{3+}/Yb^{3+} in YAG

In Fig. 6 we show a MMCT configuration coordinate diagram of Ce^{3+}/Yb^{3+} in YAG, which results from representing Eq. 34 along the ground state electron transfer reaction coordinate defined by Eqs. 26, 27, and 32. The representation along the $Ce^{3+}(5d_1^1)$-$Yb^{3+}(^2F_{7/2}) \rightarrow Ce^{4+}$-$Yb^{2+}$ reaction coordinate in the same scale is hard to distinguish at sight. We used the following data: (1) The $E_{D_iA_j,e}$=$E_e(Ce_i^{3+}$-$Yb_j^{3+})$ energy offsets were obtained from the experimental excitation energies of Ce^{3+} and Yb^{3+}, which are shown in Table I. Since we do not have empirical data on the minimum-to-minimum Ce^{3+}-to-Yb^{3+} charge transfer excitation energy, we treat it here as an empirical parameter such that it provides a diagram consistent with the experiments; we used $E_{D_0^+A_0^-,e}$=$E_e(Ce^{4+}$-$Yb^{2+})$=14000 cm^{-1}. (2) We used $d_{A_0^-}$–d_{A_0}=$d_{Yb^{2+}O}$–$d_{Yb^{3+}O}$=0.14 Å, as in Sec. III B, and d_{D_0}–$d_{D_0^+}$=$d_{Ce^{3+}O}$–$d_{Ce^{4+}O}$=0.16 Å, using the same procedure as in Yb^{2+}/Yb^{3+} (90% of the difference between the ionic radii of Ce^{3+} and Ce^{4+} in coordination 8, 1.143 Å and 0.97 Å respectively.[18]). We used the same Ce-O

distance offset in all $4f^1$ states of Ce^{3+} and a -0.02 Å offset for the lowest $5d^1$ state (Table I), slightly larger than the -0.014 Å found in *ab initio* calculations in YAG:Ce^{3+}, which has been considered to be underestimated.[23] (3) The donor and acceptor force constants are $k_D=\mu\omega_D^2$ and $k_A=\mu\omega_A^2$, with $\mu=m(\mathrm{O})=15.999$ amu. We used $\bar{\nu}_D = \omega_D/(2\pi c)=210$ cm^{-1}, which is 5% larger than the 200 cm^{-1} vibrational sequence found in Ref. 17 for YAG:Ce^{3+} (it corresponds to using a common force constant for Ce^{3+} and Ce^{4+} 10% larger than that of Ce^{3+}; the force constant is expected to be larger in Ce^{4+} than in Ce^{3+}). And we used $\bar{\nu}_A=\omega_A/(2\pi c)=310$ cm^{-1}, which is the common vibrational frequency for Yb^{2+} and Yb^{3+} that we used in Sec. III B.

In the MMCT configuration coordinate diagram, we observe the states of the Ce^{3+}-Yb^{3+} pair, which have been discussed above, and, crossing them, the ground state of the Ce^{4+}-Yb^{2+} pair, with a horizontal offset of 0.60 Å (Eq. 33). This diagram is basically consistent with the experiments and the interpretations given in Ref. 3. The lowest $Ce^{3+}(5d_1^1)$-$Yb^{3+}(^2F_{7/2})$ state can decay nonradiatively to the Ce^{4+}-Yb^{2+} MMCT state with a small energy barrier. This barrier is 73 cm^{-1} and the crossing is produced on the left side of the $Ce^{3+}(5d_1^1)$-$Yb^{3+}(^2F_{7/2})$ minimum with the above data; although the energy of the barrier can change with the parameters of the model, the basic interpretation is mantained for a relatively wide range around the present data. Next, the Ce^{4+}-Yb^{2+} MMCT state can decay directly to the $Ce^{3+}(4f^1)$-$Yb^{3+}(^2F_{5/2})$ manifold, which can yield Yb^{3+} $^2F_{5/2} \rightarrow ^2F_{7/2}$ emission. This is consistent with the observations of energy transfer from Ce^{3+} to Yb^{3+} in YAG:Ce,Yb, with its temperature dependence, and with the Yb^{3+} emission not showing rise time, so that it supports the given interpretation as due to a thermally activated decay through an intermediate Ce^{4+}-Yb^{2+} charge transfer state,[3] and complements it with a more detailed description. A value of $E_e(Ce^{4+}\text{-}Yb^{2+})$ around 2000 cm^{-1} higher is also consistent with the experiments: e.g. a value of 16000 cm^{-1} gives a 30 cm^{-1} barrier and a crossing on the right side of the minimum. Note that, according to Eq. 25, several $E_e(Ce^{4+}\text{-}Yb^{2+})$ values associated to different Ce-Yb distances can coexist in the material.

An additional interesting feature was observed in the experiments of Ref. 3: The intensity of the Yb^{3+} $4f\rightarrow4f$ emission as excited with the Ce^{3+} $4f\rightarrow5d$ absorption strongly decreases above 110 K, after the initial increase with temperature due to the thermally activated crossing to the Ce^{4+}-Yb^{2+} MMCT state. The crossing between the Ce^{4+}-Yb^{2+} MMCT state and the lowest $Ce^{3+}(4f^1)$-$Yb^{3+}(^2F_{7/2})$ manifold was suggested as a possible explanation. The present MMCT configuration coordinate diagram does not rule out such an explanation because the crossing exists, although it has a relatively high barrier (590 cm^{-1} with the present data). However, the consideration of both the MMCT diagram of Ce^{3+}-Yb^{3+} in YAG (Fig. 6) and the IVCT diagram of Yb^{2+}-Yb^{3+} in YAG (Fig. 4), suggests an alternative explanation: The Ce^{3+}-to-Yb^{3+} MMCT produced after the Ce^{3+} $4f\rightarrow5d$ absorption increases the probability of formation of Yb^{2+}-Yb^{3+} pairs, hence, of quenching the Yb^{3+} $4f\rightarrow4f$ emission via IVCT non-radiative decay, as discussed in Sec. III B.

V. CONCLUSIONS

Quantitative configuration coordinate diagrams for intervalence charge transfer states of mixed valence pairs and metal-to-metal charge transfer states of heteronuclear pairs of dopant ions in solid hosts, have been introduced and discussed in detail. They are obtained with the use of vibrational frequencies and excitation energies of single-ion active centers, together with differences between ion-ligand distances of the single-ion donor and acceptor centers. These data are attainable empirically, either from direct measurements or from estimations, e.g. based on ionic radii, and they can be calculated with *ab initio* methods. The IVCT configuration coordinate diagram of Yb^{2+}/Yb^{3+} mixed valence pair in Yb-doped YAG, and the MMCT configuration coordinate diagram of Ce^{3+}/Yb^{3+} heteronuclear pair in Ce,Yb-codoped YAG, have been obtained and discussed. Empirical data of the individual ions doped in YAG have been used for this purpose.

The analysis of the Yb^{2+}/Yb^{3+} IVCT diagram suggest that quenching of the Yb^{3+} $4f \rightarrow 4f$ emission takes place by means of IVCT non-radiative decay in Yb^{2+}/Yb^{3+} pairs.

The analysis of the Ce^{3+}/Yb^{3+} MMCT diagram supports a previous interpretation of energy transfer from Ce^{3+} to Yb^{3+} in Ce,Yb-codoped YAG, after Ce^{3+} $4f \rightarrow 5d$ excitation, via a Ce^{4+}-Yb^{2+} MMCT state. The diagram provides the details of this process. The energy of the structurally relaxed Ce^{4+}-Yb^{2+} pair is estimated to lie at either about 14000 cm^{-1} or 16000 cm^{-1} above the structurally relaxed Ce^{3+}-Yb^{3+} pair. According to the diagram, there is a higher probability of nonradiative decay from the intermediate Ce^{4+}-Yb^{2+} pair to the excited $Ce^{3+}(4f^1)$-$Yb^{3+}(^2F_{5/2})$ manifold than to the ground $Ce^{3+}(4f^1)$-$Yb^{3+}(^2F_{7/2})$ manifold of the Ce^{3+}-Yb^{3+} pair. Altogether, the two diagrams suggest that the temperature quenching of the Yb^{3+} $4f \rightarrow 4f$ emission excited with Ce^{3+} $4f \rightarrow 5d$ absorption is due to the formation of Yb^{2+}-Yb^{3+} pairs after MMCT from Ce^{3+}-to-Yb^{3+} in Ce^{3+}-Yb^{3+} pairs.

Acknowledgments

This work was partly supported by a grant from Ministerio de Economía y Competitivad, Spain (Dirección General de Investigación y Gestión del Plan Nacional de I+D+I, MAT2011-24586 and MAT2014-54395-P).

[1] J. W. Verhoeven, Pure Appl. Chem. **68**, 2223 (1996).
[2] G. Blasse, Struct. Bond. **76**, 153 (1991).
[3] D. C. Yu, F. T. Rabouw, W. Q. Boon, T. Kieboom, S. Ye, Q. Y. Zhang, , and A. Meijerink, Phys. Rev. B **90**, 165126 (2014).
[4] E. Pinel, P. Boutinaud, and R. Mahiou, J. Alloys Compd. **380**, 225 (2004).
[5] G. C. Allen and N. S. Hush, Prog. Inorg. Chem. **8**, 357 (1967).
[6] M. Robin and P. Day, Adv. Inorg. Chem. Radiochem. **10**, 247 (1968).
[7] W. van Schaik, S. Lizzo, W. Smit, and G. Blasse, J. Electrochem. Soc. **140**, 216 (1993).
[8] C. Wickleder, Z. Naturforsch. **57b**, 901 (2002).
[9] L. Seijo and Z. Barandiarán, J. Chem. Phys. **141**, 214706 (2014).
[10] Z. Barandiarán and L. Seijo, J. Chem. Phys. **141**, 234704 (2014).
[11] E. Loh, Phys. Rev. **184**, 348 (1969).
[12] H. Witzke, D. S. McClure, and B. Mitchell, in *Luminescence of Crystals, Molecules, and Solutions*, edited by F. E. Williams (Plenum, New York, 1973), p. 598.
[13] S. B. Piepho, E. R. Krausz, and P. N. Schatz, J. Amer. Chem. Soc. **100**, 2996 (1978).
[14] R. A. Buchanan, K. A. Wickersheim, J. J. Pearson, and G. F. Herrmann, Phys. Rev. **159**, 245 (1967).
[15] H. Przybylińska, C.-G. Ma, M. G. Brik, A. Kamińska, P. Sybilski, A. Wittlin, , M. Berkowski, Y. Zorenko, V. Gorbenko, et al., Appl. Phys. Lett. **102**, 241112 (2013).
[16] L. Seijo and Z. Barandiarán, Phys. Chem. Chem. Phys. **16**, 3830 (2014).
[17] V. Bachmann, C. Ronda, and A. Meijerink, Chem. Mater. **21**, 2077 (2009).
[18] R. D. Shannon, Acta Crystallogr. A **32**, 751 (1976).
[19] L. Seijo and Z. Barandiarán, Int. J. Quantum Chem. **60**, 617 (1996).
[20] A. Lupei, V. Enaki, V. Lupei, C. Presura, and A. Petraru, J. Alloys Compd. **275–277**, 196 (1998).
[21] P. Yang, P. Deng, and Z. Yin, J. Lumin. **97**, 51 (2002).
[22] C. W. Struck and W. H. Fonger, J. Lumin. **10**, 1 (1975).
[23] J. Gracia, L. Seijo, Z. Barandiarán, D. Curulla, H. Niemansverdriet, and W. van Gennip, J. Lumin. **128**, 1248 (2008).